Dual Charge and Vortex Superpositions in a Small Josephson Junction Array

Caspar H. van der Wal and J. E. Mooij
Department of Applied Physics and Delft Institute for Micro Electronics and Submicron Technology (DIMES), Delft University of Technology, P.O. Box 5046, 2600 GA Delft, the Netherlands
(Submitted for publication 28 March 2001)

We studied the ground state of a small two-dimensional array of Josephson junctions, in which the charging energy is comparable to the Josephson coupling energy. Measurements of the array's critical supercurrent demonstrate that dual charge and vortex superpositions coexist in the array.

PACS numbers: 74.50.+r, 73.23.Hk, 03.65.-w

Josephson junction arrays with underdamped low-capacitance junctions are model systems with non-commuting phase and number variables. The Josephson effect and single-charge effects have a competing influence on the array's ground state. We present an experiment on a small two-dimensional array that has a self-dual geometry: It can be described as two coupled islands with a high charging energy, but also as two coupled loops that can each contain a vortex (Fig. 1a). We succeeded in having experimental control over all magnetic and charge frustrations (Fig. 2). This allowed for a study of the array's quantum mechanical ground state, and our results demonstrate that charge and vortex superpositions occur in the array in a dual fashion.

We measured the array's critical supercurrent as a function of charge and magnetic frustration, symmetrically applied to both islands or loops. The charge frustration n_g of the two islands was controlled with capacitively coupled gate electrodes. The array's magnetic frustration $f = \Phi/\Phi_0$ was set by applying a magnetic flux Φ to the loops (Φ_0 is the flux quantum). The critical current as a function of n_g showed a periodic modulation with two maximums per period (Fig. 3a). The period corresponds to inducing a charge $2e$ on the islands. As a function of f we observed a periodic modulation with two minimums per period (Fig. 3b), and the period corresponds to applying a flux quantum to each loop. In the n_g window between the maximums in Fig. 3a, the array has two different but degenerate charge configurations that are stable (one excess Cooper pair on the top island, or one on the bottom island in Fig. 1a). Similarly, in the f window between the minimums in Fig. 3b the array has two different stable phase configurations (a vortex in the left or the right loop), that are also degenerate. We will show that a study of the positions of the maximums and minimums in the critical current (Fig. 4) yields information about the array's ground state, and that this can be used to demonstrate superpositions of the degenerate charge and vortex states.

Until now superposition states have only been demonstrated in the most rudimental Josephson junction systems. Superpositions of single-charge states have been observed in systems with a single island [1–3], but such systems do not have multiple stable vortex configurations. In single loops with Josephson junctions, superpositions of persistent-current states have been demonstrated [4], but these systems are insensitive to the background charges and the two current states do not correspond to vortices at different geometric positions in an array. Our array has both charge and vortex characteristics, and our experiment links superconducting single-charge effects with vortex physics in larger arrays. In these larger systems, a small magnetic field induces vortices that behave as particles. The array's total Josephson energy is minimized for a certain distribution of vortices, where each vortex has a well-defined position. The charging energy, on the other hand, favors a state with a well-defined number of Cooper pairs on each island, in which the charges are localized and the junction phases have large quantum fluctuations. Background charges polarize each island, and this determines which Cooper-pair distribution has the lowest energy. The duality between these two pictures has drawn much attention (for a recent review see [5]). It has been supported by the observation of superconductor-to-insulator transitions, and several localization and quantum-interference effects in two-dimensional and quasi-one-dimensional arrays [5]. However, these studies have been limited by the fact that the charging effects could not be fully controlled: The background charges are in practice strongly disordered, and charge configurations with unpaired quasiparticles usually play a role.

We present results from three arrays, denoted by 1–3 (the same arrays and numbering as in Ref. [6], where experimental details have been reported). The islands are coupled to each other and to macroscopic leads by identical junctions that have Josephson coupling $E_J = \frac{\hbar}{2e} I_{co}$ and charging energy $E_C = e^2/2C$ (where I_{co} the critical current and C the capacitance of the junctions). We estimated E_J and E_C from the current-voltage characteristic and electron-microscope inspection [6]. Microwave spectroscopy yielded a better estimate for C for arrays 2 and 3 [7]. Array 1 had $E_J = 71\,\mu$eV and $E_J/E_C = 0.48 \pm 0.1$. Array 2 and array 3 (fabricated on the same chip and nominally identical) had $E_J = 31\,\mu$eV and $E_J/E_C = 0.27 \pm 0.03$. Measurements on array 3 were

most accurate, and we will emphasize these results.

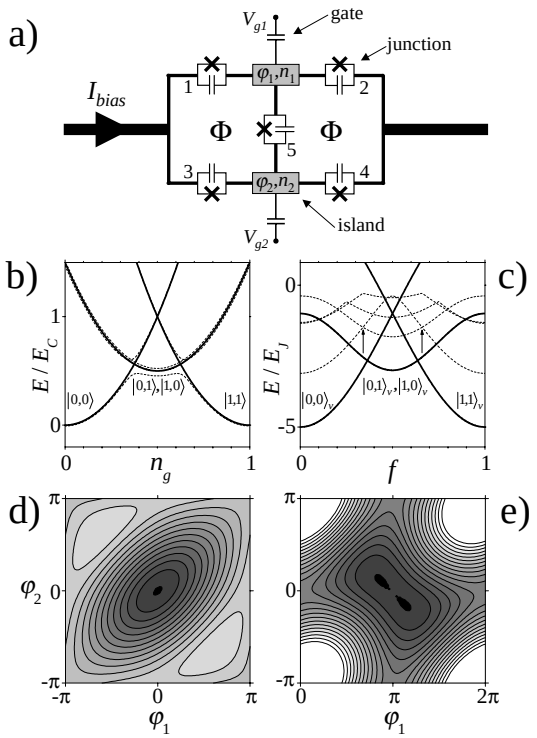

FIG. 1. a) Schematic of the array. The Josephson junctions are modelled by the parallel combinations of the Josephson tunnel element (cross) and the junction capacitance. A bias current I_{bias} can be injected from macroscopic leads. b) The array's electrostatic energy vs. n_g (solid). The dashed lines are examples of eigen energies calculated for $E_J/E_C = 0.05$, $f = 0$ and $I_{bias} = 0$. c) The array's total Josephson energy vs. f (solid). The dashed lines are eigen energies calculated for $E_J/E_C = 2$, $n_g = 0$ and $I_{bias} = 0$. The arrows show that the distance between the level crossings is larger for the quantum levels. In d) and e) the total Josephson energy U_J vs. φ_1 and φ_2, on the same gray scale (black is low U_J). The plots are for $f = 0.364$, $I_{bias} = 0$, and $\delta = 0$ (d), and $\delta = \pi$ (e).

The arrays had Al-Al_2O_3-Al tunnel junctions and were fabricated with e-beam lithography and shadow-evaporation techniques. The junctions had an area of about $0.015\,\mu\mathrm{m}^2$ and $C \approx 0.7\,\mathrm{fF}$. The loops had an area of $1\,\mu\mathrm{m}^2$. Measurements were carried out in a dilution refrigerator with rfi-feedthrough filters at room temperature and copper-powder filters at the temperature of the sample (10–70 mK). The arrays were current-biased (I_{bias}) in a low-impedance environment with a small but non-vanishing damping. The current-voltage characteristic had a clear supercurrent branch (Fig. 2a) , and the bias current I_{SW} where it switches from the supercurrent branch was used as a measure for the theoretical value of the array's critical supercurrent I_C [1].

Measurements of I_{SW} as a function of the voltages on the two gate electrodes showed a modulation that was $2e$ periodic in the induced charges (Fig. 2b). This shows that unwanted parity effects from unpaired quasiparticles were almost completely suppressed [6]. Previous studies of small two-dimensional arrays were hindered by these parity effects [8]. The observed honeycomb pattern in Fig. 2b was used to tune the gates to values where they compensate the influence of background charges in the tunnel barriers or the substrate with an accuracy of about 1 % [6]. The charge frustration n_g is thus defined as $n_g = C_g(V_g - V_{off})/2e$, where $C_g \ll C$ the gate capacitance, V_g the voltage on the gate electrode, and V_{off} the gate voltage that compensates the influence of background charges. We will concentrate here on symmetrically polarized islands, $n_{g1} = n_{g2}$, denoted by n_g. The critical current is periodic with period 1 in f and n_g, and we will therefore restrict ourselves to frustration values between 0 and 1.

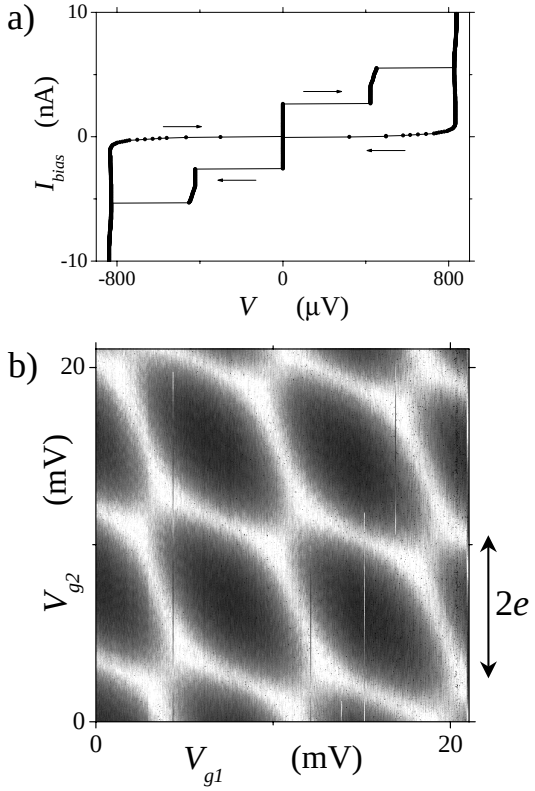

FIG. 2. a) Current-voltage characteristic of the array. Arrows indicate the direction of the hysteretic cycle. b) Gray scale plot of switching currents I_{SW} vs. gate voltages V_{g1} and V_{g2}, measured with $f = 0$ on array 3 (black is 0 nA, white is 6 nA, 250.000 switching events). The I_{SW} modulation is $2e$ periodic in the induced gate charges.

The array's Hamiltonian is the sum of the Josephson and electrostatic energies and has been worked out by Lafarge *et al.* [9]. The two loops have a very small self inductance, such that the fluxoid-quantization conditions for each loop act as constraints on the junctions' gauge-invariant phase coordinates γ_i. The system has three degrees of freedom and we use generalized coordinates that are sum and difference coordinates of the

junction phases: $\varphi_1 = \frac{1}{2}(\gamma_1 - \gamma_2)$, $\varphi_2 = \frac{1}{2}(\gamma_3 - \gamma_4)$ and $\delta = \frac{1}{2}(\gamma_1+\gamma_2+\gamma_3+\gamma_4)$, with the junctions numbered as in Fig. 1a (the direction of positive current is in each branch from left to right or from top to bottom). These variables have conjugate charge coordinates with commutation relations $[\varphi_1, n_1] = i$, $[\varphi_2, n_2] = i$ and $[\delta, k] = i$. Here n_1 and n_2 are the number of excess Cooper pairs on the top and bottom island respectively, and k is the number of Cooper pairs that has been transferred through the array. The phase δ can thus be considered as the phase difference across the array, and φ_1 and φ_2 can be considered the phases of the two islands. The array's low-impedance environment with small damping causes δ to behave like a classical phase coordinate. The island coordinates have underdamped dynamics, and due to the low island capacitance both the charges (n_1, n_2) and the phases (φ_1, φ_2) are quantum variables. The bias current is related to δ by $I_{bias} = \frac{2e}{\hbar}\frac{\partial E_g}{\partial \delta}$, where E_g is the array's ground-state energy. I_C is the maximum of I_{bias} with respect to δ, and a measurement of I_C thus provides information about the ground state.

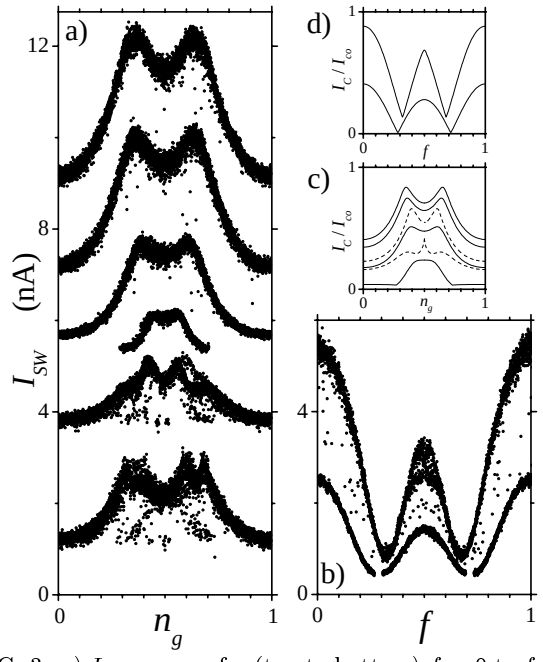

FIG. 3. a) I_{SW} vs. n_g, for (top to bottom) $f = 0$ to $f = 0.5$ in steps of 0.1 (data 7 nA, 5.5 nA, 5 nA, 5 nA, 3 nA and no offset). b) I_{SW} vs. f, for $n_g = 0.36$ (top, 0.25 nA offset) and $n_g = 0$ (bottom, no offset). Data from array 3. The data points with low I_{SW} where $n_g \approx \frac{1}{2}$ and $f \approx \frac{1}{2}$ are due to residual parity effects [6]. Data points for very low I_{SW} are absent since they could not be recorded. In c) and d) simulated I_C in units of I_{co} for $E_J/E_C = 0.27$. Solid lines in c) are for (top to bottom) $f = 0$, 0.1, 0.2, 0.3, and dashed (bottom to top, -0.05 offset) for $f = 0.4$, 0.5. In d) curves for $n_g = 0$ (bottom) and 0.36 (top, 0.05 offset).

Measurements of I_{SW} as a function of n_g (Fig. 3a) show a minimum at $n_g = 0$. At this point the array's electrostatic free energy E_{el} is lowest for the charge state $|n_1, n_2\rangle = |0, 0\rangle$ (if the array is in the zero-voltage state it is independent of k). This state is coupled to consecutive charge states, which allows for a supercurrent to flow. However, other charge states have a higher E_{el} (Fig. 1b), and charge fluctuations are suppressed. Here the Coulomb blockade of the supercurrent [10,1,2] is most effective and causes the minimum in I_{SW}. When increasing n_g from 0 to 1, the charge state with lowest E_{el} is first $|0,0\rangle$, then $|0,1\rangle$ and $|1,0\rangle$ (degenerate), and near $n_g = 1$ it is $|1,1\rangle$ (solid lines in Fig. 1b). For $C_g \ll C$ the transitions are at $n_g = \frac{3}{8}$ and $n_g = \frac{5}{8}$. Near these points the Coulomb blockade effects are minimal and there are maximums in I_{SW}. More interestingly, near the maximums the array switches from having a single state $|n_1, n_2\rangle$ with the lowest E_{el}, to a situation where two degenerate charge states have the lowest E_{el}. The ground state should be very sensitive to such a transition since it is a superposition of states $|n_1, n_2\rangle$ with the highest amplitudes for the $|n_1, n_2\rangle$ with lowest E_{el} [10,1,2].

We observed that the positions of the maximums in I_{SW} versus n_g depend on f. The positions of the maximums are the result of a competition between two effects. For n_g values around $n_g = \frac{1}{2}$, the ground state is close to the form $(|0,1\rangle+|1,0\rangle)/\sqrt{2}$, and has an eigen energy that is about $E_J/2$ lower than E_{el} due to the coupling of the central junction. Increasing E_J of the central junction results therefore in a larger n_g window where the ground state is of this form, and the distance between the maximums becomes larger as well. On the other hand, these two charge state are also coupled to the $|0,0\rangle$ and $|1,1\rangle$ states by the junctions 1–4. This results in the level repulsion at $n_g = \frac{3}{8}$ and $n_g = \frac{5}{8}$, as in Fig. 1b. Increasing E_J of the junctions 1–4 enhances the level repulsion, which causes the maximums in E_g to approach $n_g = \frac{1}{2}$ or to merge into one maximum. The maximums in I_C follow this pattern. For our array, the two effects are in balance for $f = 0$ (Fig. 3a). Increasing f from zero induces a persistent current in the array that flows through the outer branches of the array, i. e. through junctions 1–4, but not through the central junction. The switching current measures the array's ground state at finite bias current. The combination of I_{bias} and the persistent current breaks the symmetry in the effective Josephson coupling for the top and the bottom island. For the bottom island, the bias current is compensated by the persistent current, while for the top island the bias current and the persistent current add up and reduce the effective Josephson coupling $-E_J \cos\gamma_i$ of junction 1 and 2. The overall effect is that the array has a lower I_{SW} due to the weak effective E_J in the upper branch, but that the strong coupling in the lower branch causes the two maximums to merge into a single maximum with increasing f. Around $f = 0.3$ a vortex enters the array (see also below), and at $f = 0.5$ the symmetry is restored since the flux-induced currents now lead to an equal reduction

of the effective E_J for the two islands. Numerical calculations (as described in [9,11]) of I_C (Fig. 3c) and the positions $n_{g\,max}$ of the maximums (Fig. 4a) agree very well with the measurements for $f \lessapprox 0.35$. For $f \gtrapprox 0.35$, the I_{SW} data is less reliable due to residual parity effects [6] that suppress I_{SW} at places where the maximums are expected (lower two traces in Fig. 3a).

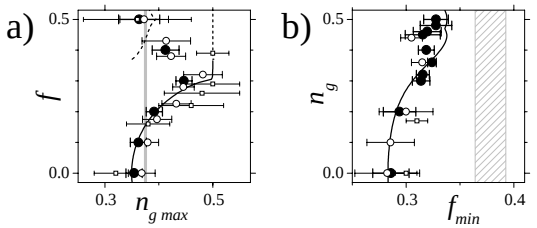

FIG. 4. Measured and simulated positions of maximums in I_{SW} vs. n_g, and minimums in I_{SW} vs. f. Data from array 1 (squares), 2 (open circles) and 3 (solid circles). Errors bars indicate the uncertainty in absolute positions of maximums and minimums, uncertainty in the shifts of positions in one measured trace with respect another is about one order smaller. In a) positions of maximums $n_{g\,max}$ from data as in Fig. 3a, for different f. In b) positions of minimums f_{min} from data as in Fig. 3b, for different n_g. Solid black lines show simulated values for $E_J/E_C = 0.27$, the black dashed parts in a) represent the fact that I_C develops for $f \gtrapprox 0.37$ an additional peak structure. Gray areas indicate where $n_{g\,max}$ and f_{min} are expected for classical charging and Josephson effects.

Similarly, the critical current as a function of f was studied. We will first analyze the case with $I_{bias} = 0$. For $f = 0$, the array's total Josephson energy U_J is lowest for $|\delta, \varphi_1, \varphi_2\rangle = |0, 0, 0\rangle$ (Fig. 1c,d). This corresponds to a phase configuration without vortices in the array, and it will be denoted as $|0,0\rangle_v$. When increasing f from 0 to 1, the phase configuration with lowest U_J is for $0.364 < f < 0.636$ one of the two degenerate states $|\delta, \varphi_1, \varphi_2\rangle = |\pi, \pi \pm (f - \frac{1}{2})\pi, \mp(f - \frac{1}{2})\pi\rangle$, as indicated by the solid lines in Fig. 1c and the double-well potential in Fig. 1e (equivalent solutions exist for $\delta = -\pi$, the classical behavior of δ enforces one of the two cases). These states with $\delta = \pi$ correspond to phase configurations with a single vortex in the array [9], i. e. with a vortex in the right or the left loop. In Fig. 1c these two states are denoted as $|0,1\rangle_v$ and $|1,0\rangle_v$. For $f > 0.636$, the array returns to a vortex-free phase configuration with $\delta = 0$, but now with about one flux quantum induced in each loop, and this state can thus be denoted as $|1,1\rangle_v$. At points close to $f = 0.364$ and $f = 0.636$, the band E_g versus δ has minimum amplitude, and δ can easily make multiple transitions of π. This leads to minimums in I_{SW} (Fig. 3b).

In the f window around $f = \frac{1}{2}$, the underdamped quantum behavior of φ_1 and φ_2 allows for tunnelling between the two classical solutions at the minimums in U_J in Fig. 1e. Moreover, comparison with U_J in Fig. 1d shows that φ_1 and φ_2 are here less confined. The f window in which the array's ground-state energy with $\delta = \pi$ is lower than that for $\delta = 0$ is therefore expected to be wider than the classical boundaries $f = 0.364$ and $f = 0.636$, see also Fig. 1c (for finite bias currents the classical boundaries move towards $f = \frac{1}{2}$, up to $f = 0.393$ and $f = 0.607$ for $I_{bias} = I_C$). The minimums in Fig. 3b are clearly further apart than expected classically. Moreover, the positions of the minimums f_{min} depend on n_g. Due to the classical behavior of δ (i. e. no coherent coupling to a vortex reservoir outside the array) we can interpret the positions of the minimums here directly as the point where the array makes the transition between a ground state without a vortex in the array and a ground state that is a superposition of the $|0,1\rangle_v$ and $|1,0\rangle_v$ state. A shift of the f_{min} corresponds to a shift of the position of this transition.

The shift of f_{min} is analyzed in a picture where the state of the array is analogous to a particle in a two-dimensional periodic potential [10]. The U_J in Fig. 1d is a unit cell for $\delta = 0$ and Fig. 1e for $\delta = \pi$. The influence of n_g becomes evident in a tight-binding description. This has been worked out in Ref. [11] for a system with a similar Hamiltonian. For $\delta = \pi$ the terms that couple one of the classical solutions with neighboring states is of the form $-t_1 - \sum_j t_2 e^{i\mathbf{k}\cdot\mathbf{a}_j}$, where t_1 the coupling from intra-unit cell coupling, and the sum over terms t_2 for inter-unit cell coupling. The length of the $\mathbf{k}$ vector is equal to n_g, and $\mathbf{a}_j$ is the position vector to the nearest-neighbor site. For $\delta = 0$, as in Fig. 1d, there is only inter-unit cell coupling. The coupling terms to the nearest-neighbor states are $-\sum_j t_3 e^{i\mathbf{k}\cdot\mathbf{a}_j}$. The $\delta = \pi$ ground state will have a minimum energy for $n_g = 0$. Non-integer values of n_g cause a phase difference between t_1 and inter-unit cell coupling, and lead to a higher eigen energy. As a result the f window where $\delta = \pi$ becomes smaller. This effect dominates the shift in f_{min} since the array has $t_1 > t_2 > t_3$. For $n_g \approx \frac{3}{8}$, where Coulomb blockade effects are minimal, the minimums have moved in the direction where f_{min} is expected for classical behavior. An analysis with finite bias current is more tedious, but the overall picture remains valid. Numerical calculations of I_C (Fig. 3d) and the positions of the minimums f_{min} (Fig. 4b) agree again very well with the observations. From the observed positions and shifts of f_{min} we conclude that the array has around $f = \frac{1}{2}$ a ground state that is a superposition of two vortex states.

The authors thank P. Lafarge, M. H. Devoret, K. K. Likharev, T. P. Orlando, Y. Nakamura, P. Hadley, R. N. Schouten and C. J. P. M. Harmans for fruitful discussions, and the Dutch FOM for financial support.

[1] P. Joyez *et al.*, Phys. Rev. Lett. **72**, 2458 (1994).
[2] M. Matters, W. J. Elion, and J. E. Mooij, Phys. Rev. Lett. **75**, 721 (1995).

[3] Y. Nakamura, Yu. A. Pashkin, and J. S. Tsai, Nature **398**, 786 (1999).
[4] J. R. Friedman *et al.*, Nature **406**, 43 (2000); C. H. van der Wal *et al.*, Science **290**, 773 (2000).
[5] R. Fazio and H. S. J. van der Zant, to be published in Phys. Rep. (2001); cond-mat/0011152.
[6] C. H. van der Wal and J. E. Mooij, J. Supercond. **12**, 807 (1999).
[7] C. H. van der Wal, P. Kuiper, and J. E. Mooij, Physica B **280**, 243 (2000). These results were measured on array 2 at a later stage. During sample storage the junction resistance had increased from 21 kΩ to 28 kΩ.
[8] W. J. Elion, J. J. Wachters, L. L. Sohn, and J. E. Mooij, Phys. Rev. Lett. **71**, 2311 (1993); V. Bouchiat, Ph. D. thesis, Université Paris 6, 1997.
[9] P. Lafarge, M. Matters, and J. E. Mooij, Phys. Rev. B **54**, 7380 (1996). We found a missing factor 2 in the numerical code used for this article, the figures are for $E_J/E_C = 0.4$ instead of $E_J/E_C = 0.2$.
[10] D. V. Averin and K. K. Likharev, in *Mesoscopic Phenomena in Solids*, edited by B. L. Al'tshuler, P. A. Lee, and R. A. Webb (Elsevier, Amsterdam, 1991), Chap. 6.
[11] T. P. Orlando *et al.*, Phys. Rev. B **60**, 15398 (1999).